New Paradigm for Turbulent Transport Across a Steep Gradient in Toroidal Plasmas

H. S. Xie,[1,*] Y. Xiao,[1,†] and Z. Lin[2,3]
[1]Institute for Fusion Theory and Simulation, Department of Physics, Zhejiang University, Hangzhou 310027, People's Republic of China
[2]Department of Physics and Astronomy, University of California, Irvine, California 92697, USA
[3]Fusion Simulation Center, School of Physics, Peking University, Beijing 100871, China
(Received 30 August 2016; revised manuscript received 6 January 2017; published 1 March 2017)

First principles gyrokinetic simulation of the edge turbulent transport in toroidal plasmas finds a reverse trend in the turbulent transport coefficients under strong gradients. It is found that there exist both linear and nonlinear critical gradients for the nonmonotonicity of transport characteristics. The discontinuity of the transport flux slope around the turning gradient shows features of a second order phase transition. Under a strong gradient the most unstable modes are in nonground eigenstates with unconventional mode structures, which significantly reduces the effective correlation length and thus reverse the transport trend. Our results suggest a completely new mechanism for the low to high confinement mode transition without invoking shear flow or zonal flow.

DOI: 10.1103/PhysRevLett.118.095001

With the input power increasing, a sudden transport "phase" with the formation of an edge transport barrier is found experimentally in fusion plasmas [1], which is called the high (H) confinement mode to distinguish it from the conventional low (L) confinement mode, where no steep gradients exist in the plasma profiles. Transport barriers, also recognized in other systems, such as in geophysical and atmospheric sciences [2], can be universal and important. The H-mode plasma stores twice as much energy as that of the L mode, thus enabling high fusion gain. The H-mode is the baseline operation scenario of the International Thermonuclear Experimental Reactor (ITER) [3]. The L-H transition involves a discontinuous change of the transport characters, and the underlying mechanism remains elusive [4]. The transition between the multiple equilibrium states resembles the continuous (or second order) phase transition of Landau [5], a critical phenomenon widely existing in nature. An improved understanding of the transition physics is not only important for fusion plasmas, but it also leads to a new paradigm for the nonlinear physics in the laboratory and the Universe.

Several theories have been proposed for the transport characteristic change [6–9] or the sudden L-H transition [10,11], where shear or zonal flow is generally invoked. But none of these theories has been fully verified by first principles simulations or validated by fusion experiments. In addition, due to many inherent *ad hoc* assumptions on the kinetic physics, these theories may only be qualitatively correct. Recently, several fluid models (cf. Ref. [12]) have also produced some of the essential features of the L-H transition; i.e., two transport "phases" are found by increasing the input power. These fluid simulation results may not be conclusive due to overlooking essential kinetic physics. A fully kinetic simulation of the L-H transition is still precluded due to the multiple temporal and spatial scale nature of the problem. The gyrokinetic simulation is so far still one of the best tools to study kinetic physics for the edge plasmas, although the validity of gyrokinetics under strong gradients is still under active research. When studying low frequency drift wave turbulence in the tokamak edge, the gyrokinetics [13] may still be valid for $R/L_T \sim 100$, where $\rho_i/L_T \sim 0.1$, satisfying the gyrokinetic assumption $\rho_i/L_T \ll 1$. In this work, we only consider electrostatic drift wave turbulence by varying density and temperature gradients while fixing the density and temperature in the simulation. Our gyrokinetic simulation [13,14], using the GTC code [15,16], shows that both the linear and nonlinear physical characteristics change nonmonotonically with a turning point at some critical gradient, which divides the gradient space into a weak gradient region (L-mode) and a strong gradient region (H-mode). It is known that drift wave turbulence can lead to anomalous transport [17]. It is also commonly accepted that stronger gradients lead to higher transport coefficients [18,19]. Based on large scale global gyrokinetic simulations using the GTC code, we report here for the first time that the turbulent transport coefficients in toroidal plasmas can be reversed under a strong gradient; i.e., a larger gradient leads to a smaller transport coefficient. The slope of the transport flux also shows a discontinuous change around the turning gradient, similar to the second order phase transition of Landau [5]. The underlying physics is found to be closely related to the unconventional mode structure under strong gradients, which significantly reduces the radial correlation length. These novel findings may suggest a completely new mechanism for the L-H transition without invoking shear flow or zonal flow.

The GTC code is a well-benchmarked global gyrokinetic particle simulation code [15,20–22], suitable for simulating

both electrostatic and electromagnetic drift wave turbulence [17]. In the low beta limit, we only use the electrostatic capability of the GTC code. The simulation parameters are taken from typical H-mode experiments of the HL-2A tokamak [23,24] using deuterium as the ion species, with an on-axis toroidal magnetic field $B_0 = 1.35T$, minor radius $a = 40$ cm, major radius $R_0 = 165$ cm, safety factor $q = 2.7$, magnetic shear $s = 0.5$, plasma temperature $T_e = T_i = 200$ eV, and plasma density $n_e(r) = n_i = 4.0 \times 10^{12}$ cm^{-3}. Assuming that the time scale for electron-ion energy exchange is shorter than the profile relaxation time scale, in the simulation we set the plasma profile gradients as $R_0/L_{T_i} = R_0/L_{T_e} = R_0/L_n$, where L_{T_i}, L_{T_e}, and L_n are the scale lengths for ion temperature, electron temperature, and particle density, respectively, i.e., $L_T^{-1} \equiv -d \ln T/dr$. Therefore, we keep $\eta = L_n/L_T = 1$ throughout this article. We note that one of the most important parameters is the peaking gradient [23]. In addition, a circular cross section is assumed for the equilibrium magnetic flux surface.

Using the preceding experimental parameters, we carry out a series of turbulence simulations by scanning the plasma profile gradients. In the simulations, we use a number of grids $150 \times 1200 \times 32$ in the radial, poloidal, and parallel directions, respectively, which leads to a grid size of $\sim 0.5\rho_i$, and 50 ions/electrons per cell to reduce the numeric noise. A larger number of grids and more particles per cell are used, and a satisfactory convergence can be obtained for the simulation results. Zero boundary conditions are used at $r = 0.7a$ and $1.0a$. The time history of the volume averaged turbulent heat conductivity and particle diffusivity is shown in Figs. 1(a)–1(c) for three strong gradients, $R_0/L_T = 30$, 50, 100, where the heat conductivity χ_j is defined by the heat flux $q_j = \int dv^3(\frac{1}{2}m_j v^2 - \frac{3}{2}T_j)\delta v_E \delta f_j \equiv n_j \chi_j \nabla T_j$, $j = i$, e, and the particle diffusivity D_j is defined by the particle flux $D_j = \int dv^3 \delta v_E \delta f_j$, with v_E the $E \times B$ drift caused by turbulence. As shown in Fig. 1, both heat conductivity and particle diffusivity decrease with the temperature gradient in the strong gradient region. This is contradictory to the common knowledge that stronger gradients lead to higher transport coefficients [18]. This phenomenon is further illustrated in Fig. 2(a) by comparing the electron diffusivity for different gradients, where the diffusivity is obtained by the time average of the saturated value in the nonlinear stage before the quasilinear flattening of the plasma profile occurs. The electron diffusivity first increases with the gradient, which is consistent with previous studies [18]. However, when we continue to increase the gradient after some critical value, as shown in Fig. 1, stronger gradients lead to lower particle diffusivity. The pink dashed line follows the conventional trend by artificial extrapolation [18]. This reverse trend of the transport coefficients also holds for ion and electron heat transport, which can be seen in Fig. 1(a) or 1(b). We note that this is the first time that such extraordinary behavior is observed for the turbulent transport under a strong gradient. In Fig. 2(b) for the electron flux vs R_0/L_T, a turning point for the gradient drive appears, and the particle flux reaches a saturation level, or increases much more slowly, when the gradient is beyond the turning point, clearly showing a discontinuous change of the slope of the particle flux. This provides strong evidence for the formation of a gradient transport barrier, even though no bifurcation occurs. If one adds more power to the core plasma than the pedestal can exhaust, the L-H transition can occur due to the gradient transport barrier, which could explain the mystery of the L-H transition; namely, the input power should exceed a certain level in order to trigger the L-H transition.

Next we examine the zonal flow effect on the nonlinear physics under a strong gradient. A previous study using the GTC code has shown that for the TEM mode the zonal flow can reduce the turbulent transport significantly ($> 50\%$)

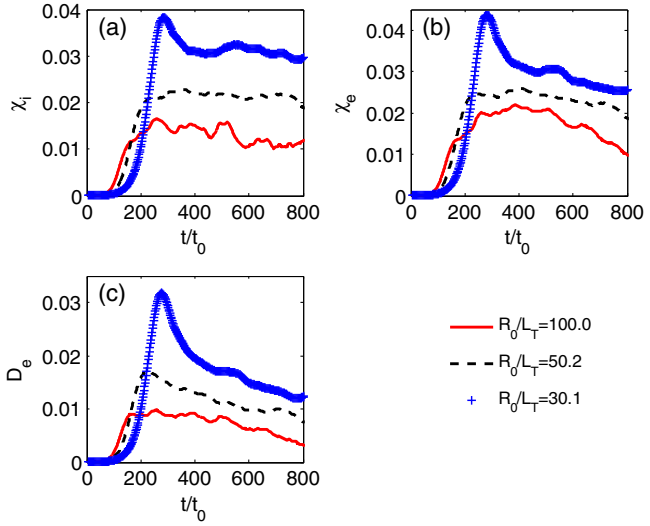

FIG. 1. Time history for three volume averaged physical quantities: (a) ion heat conductivity, (b) electron heat conductivity, and (c) electron particle diffusivity under three strong temperature gradients, where $t_0 = 0.002c_s/R_0$ is the time step size.

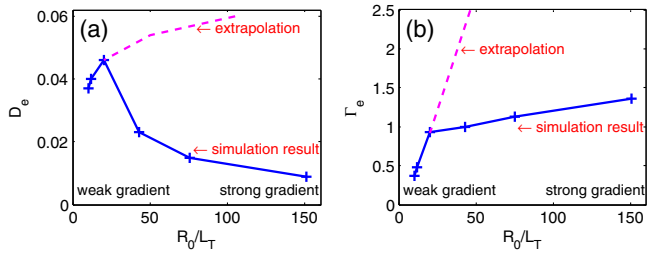

FIG. 2. (a) Time averaged electron particle diffusivity and (b) electron particle flux for different temperature gradients. A turning point (critical gradient) is found for the trend of the transport coefficients.

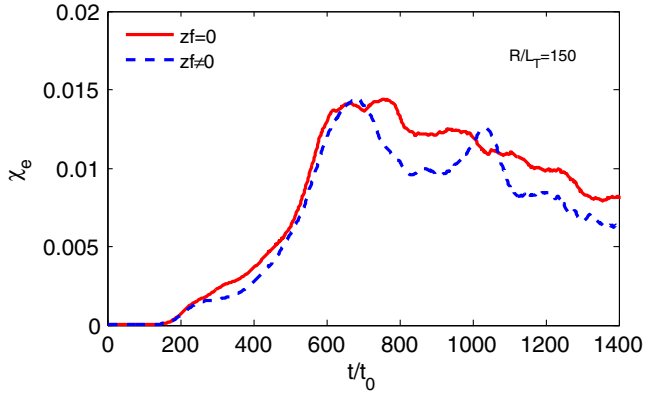

FIG. 3. Time history of electron heat conductivity in the nonlinear gyrokinetic simulation is shown for two cases under strong gradients: with and without zonal flow. The blue dashed line represents simulation with zonal flow self-consistently generated. For the red solid line, the zonal flow is artificially removed from the simulation.

under a weak gradient ($R_0/L_T = 6.9$) [21]. However, under a strong gradient, Fig. 3 shows that the zonal flow has little effect on regulating turbulence. The weak importance of zonal flow near the edge is also reported in a recent H-mode experiment by Ref. [25].

The preceding nonlinear results in Figs. 2 and 3 can be further understood by a random walk model; i.e., the transport coefficients such as the particle diffusivity D agree with $D \sim l_c^2/\tau_c$, where l_c is the correlation length and τ_c is the correlation time. By linking l_c with the characteristic perpendicular wavelength and τ_c with the linear growth rate, a simplest model of this type gives $D \sim (\gamma_k/k_\perp^2) \propto \gamma_k$. A rough estimate for the linear growth rate gives $\gamma_k \propto \nabla T$; thus, we have $D \propto \nabla T$, which leads to the Taroni-Bohm model [26]. However, this model breaks down for large gradients, as shown in Fig. 2, as the linear growth rate γ_k (inverse of the correlation time τ_c) does not increase much with the gradient (see Fig. 6). On the other hand, the correlation length l_c should be reduced dramatically in the strong gradient region, as implied by Fig. 1. Figure 4 shows two typical eddy sizes for the nonlinearly strong gradient ($R_0/L_T = 30$) and the nonlinearly weak gradient ($R_0/L_T = 10$). The zonal flow is excluded in these simulations to manifest the turbulence mode structure. We can see clear streamer structures for the case with $R_0/L_T = 10$, which shows elongated radial eddies in Fig. 4(a) and hence a large radial correlation length. The zonal flow can cut through and stretch these streamer structures and therefore effectively reduce the transport. However, under a stronger gradient $R_0/L_T = 30$, the eddy size becomes smaller and zonal flow may no longer cut through them, which can minimize the regulation effect of the zonal flow, as shown in Fig. 3.

The reverse trend of the transport coefficient in the strong gradient region can be reasonably explained by the smaller eddy size and hence smaller correlation length, which could possibly be induced by the unconventional mode structures of nonground eigenstates of micro-instabilities [27]. To examine the physics mechanism for this reverse transport trend under a strong gradient, we thus further perform a linear simulation for the most unstable mode with toroidal mode number $n = 20$ since the discontinuous change in the nonlinear transport may be related to the discontinuity in the linear eigenmode characteristics. As shown by time history and spectrum analysis of selected unstable modes in Fig. 5 (for poloidal mode number $m = 51$), two distinct frequencies clearly coexist in the electron diamagnetic direction for the linear simulation. Suppose that the three-dimensional mode structure of the electrostatic potential is represented by the Fourier series $\delta\phi(r,\theta,\zeta,t) = e^{in\zeta - i\omega t}\sum_m \delta\phi_m(r)e^{-im\theta}$, where $\omega = \omega_r + i\gamma$ is the mode frequency. We proceed to examine the mode frequency variation under different gradients. As shown in Fig. 6, there exists a clear frequency jump from the low frequency ($\omega_r < 3\omega_s$, $\omega_r < \gamma$) to the high frequency ($\omega_r > 10\omega_s$, $\omega_r \gg \gamma$) branch, where the normalized frequency $\omega_s = 1/t_s \equiv c_s/R_0$ and $c_s \equiv \sqrt{T_e/m_i}$. Around the critical jump gradient ($R_0/L_T \simeq 70$), two branches of the eigenmode coexist at the initial linear stage due to similar growth rates, as shown in Fig. 5. The low frequency branch shows a conventional ballooning structure localized at the outside

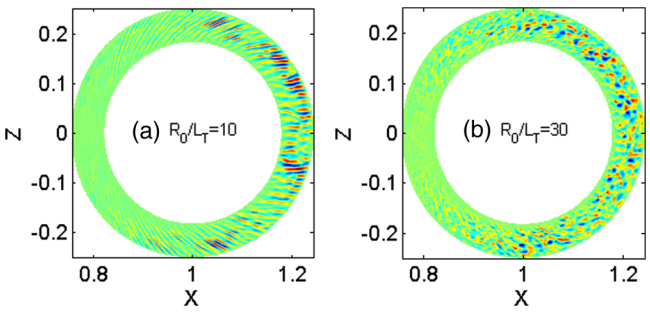

FIG. 4. Two-dimensional turbulence intensity in the poloidal plane for a nonlinearly weak gradient $R_0/L_T = 10$ and a nonlinearly strong gradient $R_0/L_T = 30$.

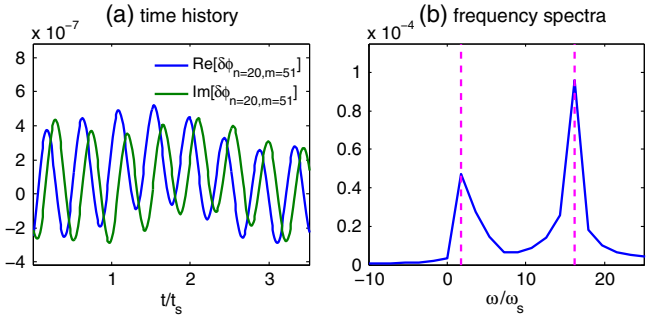

FIG. 5. (a) The time history and (b) frequency spectra for the Fourier component ($n = 20$, $m = 51$) of electrostatic potential in the linear simulation with $R_0/L_T = 75$.

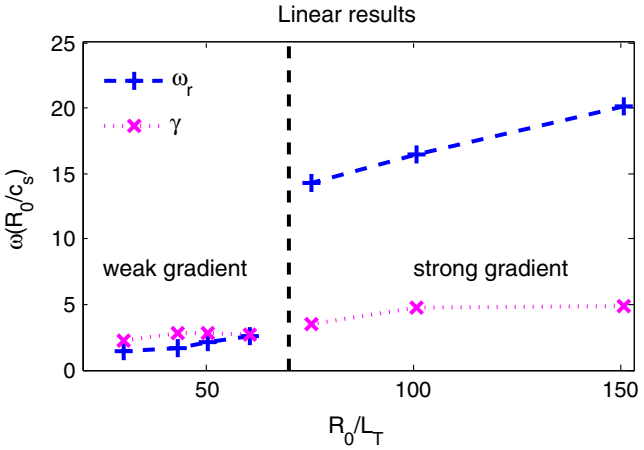

FIG. 6. Linear real frequency and growth rate for the most unstable mode under different temperature gradients using typical HL-2A parameters with selected toroidal mode number $n = 20$.

midplane (ground eigenstate), whereas the high frequency branch shows an unconventional mode structure which can localize at almost arbitrary poloidal positions or with multiple peaks (nonground eigenstate) [23,27]. For the weak gradient (L-mode), the most unstable mode is in the ground state. However, the most unstable mode can jump to the nonground eigenstate under a strong gradient (H-mode). The unconventional mode structure can significantly reduce the effective correlation length and thus the turbulent transport. This viewpoint can provide a mechanism to understand the previous nonlinear simulations in this Letter. We note the critical gradient for the frequency jump is $R_0/L_T \simeq 70$, which is around the experimental L-H transition gradient $R_0/L_T \simeq 40$–120 [24,28]. The low and high frequencies from the simulation also quantitatively agree with the characteristic frequencies of the electrostatic turbulence for typical HL-2A L-modes and H-modes, i.e., ~20 kHz and ~80 kHz, respectively [23]. The detailed linear results, especially the unconventional mode structures and eigenstate jumps, have been reported in Refs. [23,27], where the micro-instability is identified as trapped electron modes (TEMs) [29,30]. It has also been recently reported that the turbulence (usually also TEM) jumps from low frequency to high frequency during the L-H transition for experiments such as EAST [31]. Other simulations also discussed the possible important roles of the resistive ballooning mode [32] or the large diamagnetic frequency [33], but they did not show a clear sudden change of transport characteristics as the present work does.

So far we have discovered the coexistence of both linear and nonlinear critical gradients. However, the linear critical gradient ($R_0/L_T = 75$) is larger than the nonlinear critical gradient ($R_0/L_T = 25$). There could be two reasons for this difference. The first one is shown in Fig. 6: The linear growth rate ceases to grow before the linear discontinuity occurs. The second reason is associated with the following inverse poloidal spectral cascade in the nonlinear saturation

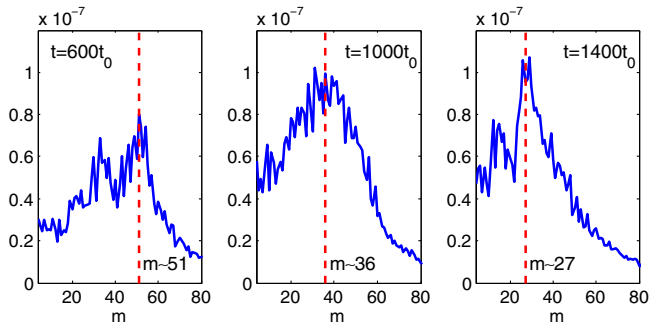

FIG. 7. The poloidal spectral cascade from high to low mode number during nonlinear saturation.

of turbulence. We carry out a nonlinear gyrokinetic simulation under a strong gradient with a typical HL-2A H-mode experimental value $R/L_T = 150$. As shown in Fig. 7, the peak m downshifts from a larger number to a smaller number during the nonlinear saturation process, which demonstrates a nonlinear inverse cascade in the poloidal spectrum. The peak m at a later saturation stage ($t = 1400t_0$, steady state, where t_0 is the time step size) is $m = 10$–40, whose value is close to the experimental value $m = 14$–33 [23,24].

In conclusion, via a first principles gyrokinetic simulation we have found a trend reversal in the transport coefficients and a discontinuous change of the slope of the transport flux in the strong-gradient regime of magnetic fusion plasmas, indicating that a small increase of the heat flux can lead to a large increase of the gradient, similar to a second order phase transition [5]. We also found that there exist both linear and nonlinear critical gradients for the discontinuity of the transport characteristics. In the linear simulation, with an increase of the edge gradient, the most unstable mode jumps from the ground eigenstate to another eigenstate. The unconventional mode structure associated with the latter can effectively reduce the correlation length and thus the transport coefficients. This result is confirmed by the nonlinear simulation, which shows that the radial correlation length is indeed reduced in the strong gradient regime, and a turning point (the nonlinear critical gradient) indeed appears in the transport coefficients. The reduction of the critical gradients and transport coefficient can be crucial to the formation of the H-mode external transport barrier as well as the L-H transition. This result therefore suggests a new pathway to the H-mode regime, namely, without the need for shear and/or zonal flows. In fact, experiments have also raised doubts about the need for the latter for the L-H transition [25,34], and the corresponding fluid models for the L-H transition are not fully convincing either [19]. Finally, we note that gyrokinetic simulations can provide quantitative outputs for closer comparison with experimental results. In fact, the critical gradient, characteristic frequency, and poloidal mode number from our nonlinear simulation are consistent with the HL-2A experiments. Moreover, for further resolving the mystery of the

L-H transition, other effects such as flow shear, electromagnetic perturbations, self-consistent evolution of the plasma profiles, etc. can also be included in the gyrokinetic simulation.

H. S. X. would like to thank D. F. Kong, G. S. Xu, and H. Q Wang for providing the experimental information from the HL-2A and EAST tokamaks. We would like to thank L. Chen, G. Y. Fu, and M. Y. Yu of ZJU, P. H. Diamond of UCSD, and X. Q. Xu of LLNL for useful discussions. This work is supported by the National Magnetic Confinement Fusion Energy Research Program under Grants No. 2015GB110000, 2015GB110003, and No. 2013GB111000, the Natural Science Foundation of China under Grant No. 11575158, the Thousand Youth Talents Plan, and the US DOE SciDac GSEP Center.

*huashengxie@gmail.com
†Corresponding author.
yxiao@zju.edu.cn

[1] F. Wagner *et al.*, Phys. Rev. Lett. **49**, 1408 (1982).
[2] C. R. Or and F. H. Busse, J. Fluid Mech. **174**, 313 (1987); M. E. McIntyre, J. Atmos. Terr. Phys. **51**, 29 (1989).
[3] K. Ikeda, Nucl. Fusion **47** (2007).
[4] F. Wagner, Plasma Phys. Controlled Fusion **49**, B1 (2007).
[5] Translated and reprinted from Landau L. D. Collected Papers (Nauka, Moscow, 1969), Vol. **1**, pp. 234–252. Originally published in Zh. Eksp. Teor. Fiz. **7**, 19 (1937).
[6] H. Biglari, P. H. Diamond, and P. W. Terry, Phys. Fluids B **2**, 1 (1990).
[7] T. S. Hahm, Phys. Plasmas **1**, 2940 (1994).
[8] R. E. Waltz, G. D. Kerbel, and J. Milovich, Phys. Plasmas **1**, 2229 (1994).
[9] J. Li and Y. Kishimoto, Phys. Rev. Lett. **89**, 115002 (2002).
[10] S. I. Itoh, K. Itoh, and A. Fukuyama, Nucl. Fusion **33**, 1445 (1993).
[11] E. J. Kim and P. H. Diamond, Phys. Rev. Lett. **90**, 185006 (2003).
[12] B. N. Rogers, J. F. Drake, and A. Zeiler, Phys. Rev. Lett. **81**, 4396 (1998); X. Q. Xu, R. H. Cohen, T. D. Rognlien, and J. R. Myra, Phys. Plasmas **7**, 1951 (2000); G. Y. Park, S. S. Kim, H. Jhang, P. H. Diamond, T. Rhee, and X. Q. Xu, Phys. Plasmas **22**, 032505 (2015); L. Chôné, P. Beyer, Y. Sarazin, G. Fuhr, C. Bourdelle, and S. Benkadda, Nucl. Fusion **55**, 073010 (2015); B. Li, C. K. Sun, X. Y. Wang, A. Zhou, X. G. Wang, and D. R. Ernst, Phys. Plasmas **22**, 112304 (2015).
[13] A. J. Brizard and T. S. Hahm, Rev. Mod. Phys. **79**, 421 (2007).
[14] W. W. Lee, J. Comput. Phys. **72**, 243 (1987).
[15] Z. Lin and T. S. Hahm, Phys. Plasmas **11**, 1099 (2004).
[16] Z. Lin, Science **281**, 1835 (1998).
[17] W. Horton, Rev. Mod. Phys. **71**, 735 (1999).
[18] A. M. Dimits *et al.*, Phys. Plasmas **7**, 969 (2000).
[19] B. Scott, Plasma Phys. Controlled Fusion **48**, B277 (2006).
[20] G. Rewoldt, Z. Lin, and Y. Idomura, Comput. Phys. Commun. **177**, 775 (2007).
[21] Y. Xiao and Z. Lin, Phys. Rev. Lett. **103**, 085004 (2009).
[22] I. Holod and Z. Lin, Phys. Plasmas **20**, 032309 (2013).
[23] H. S. Xie, Ph.D thesis, Zhejiang University, 2015.
[24] D. F. Kong *et al.*, Nucl. Fusion **57**, 014005 (2017).
[25] T. Kobayashi *et al.*, Phys. Rev. Lett. **111**, 035002 (2013).
[26] W. Horton, *Turbulent Transport in Magnetized Plasmas* (World Scientific, Singapore, 2012).
[27] H. S. Xie and Y. Xiao, Phys. Plasmas **22**, 090703 (2015).
[28] F. Ryter *et al.*, Plasma Phys. Controlled Fusion **58**, 014007 (2016); R. A. Moyer *et al.*, Phys. Plasmas **2**, 2397 (1995).
[29] B. Coppi and G. Rewoldt, Phys. Rev. Lett. **33**, 1329 (1974).
[30] P. J. Catto and K. T. Tsang, Phys. Fluids **21**, 1381 (1978).
[31] G. S. Xu *et al.*, Phys. Plasmas **19**, 122502 (2012); H. Q. Wang *et al.*, Nucl. Fusion **52**, 123011 (2012).
[32] C. Bourdelle *et al.*, Nucl. Fusion **55**, 073015 (2015).
[33] B. Scott, A. Kendl, and T. Ribeiro, Contrib. Plasma Phys. **50**, 228 (2010).
[34] S. J. Zweben, R. J. Maqueda, R. Hager, K. Hallatschek, S. M. Kaye, T. Munsat, F. M. Poli, A. L. Roquemore, Y. Sechrest, and D. P. Stotler, Phys. Plasmas **17**, 102502 (2010).